Near-Infrared Grating Couplers for Silicon Nitride Photonic Wires

Ananth Z. Subramanian, Shankar Selvaraja, *Member, IEEE*, Peter Verheyen, Ashim Dhakal, Katarzyna Komorowska, and Roel Baets, *Fellow, IEEE*

***Abstract*— Silicon nitride is a promising high-index material for dense photonic circuits and applications in the visible-midinfrared wavelength regime. Design, fabrication, and optical characterization of silicon nitride waveguides at visible-near-infrared wavelength are presented. Finally, design and experimental results are presented for the first time for linear and focused grating couplers (GCs) at near-infrared wavelength (900 nm) for plasma-enhanced chemical vapor deposition silicon nitride wires (220 × 500 nm) and compared with theoretical simulations. An experimental efficiency of 5.7 and 6.5 dB and 1-dB bandwidth of 26 and 40 nm are reported for the linear and focused GCs, respectively.**

***Index Terms*— Gratings, integrated optics, optical materials, optical waveguides.**

I. Introduction

GRATING couplers (GCs) enable efficient coupling from optical fibres to photonic integrated components (PICs) without the need of using lenses or inverted tapers [1]. They avoid expensive methods such as end-polishing and the use of lensed fibre to couple light into the waveguides, and also allows wafer-level testing of PICs. GCs with high efficiency have been successfully demonstrated for telecom wavelengths and have become a standard practice for coupling light in and out of PICs in silicon photonics [2]–[3]. GCs have also been successfully demonstrated in the telecom band in other high-index-contrast (HIC) material systems such as indium phosphide membranes [2], aluminum nitride [4], and silicon nitride (Si_3N_4)[5]. However, GCs for a HIC platform at shorter wavelengths (400–1000 nm) have not been investigated in detail. The visible and near-visible infrared (IR) bands are important for several applications such as sensing and spectroscopy [6], especially in a biological context given the high penetration depth of light in tissues in these bands. These shorter wavelengths also avoid water absorption band which helps in preventing cell damage at high powers. GC-based PICs will help in realizing efficient and easy-to-use integrated spectrometers and sensors. Si_3N_4 is a versatile HIC platform for its transparency at both visible and infrared wavelengths [7]–[9]. Besides it is compatible with the well established complementary-metal-oxide-semiconductor (CMOS) process technology thereby enabling low-cost photonic devices much like in silicon photonics.

In this letter, we present the design and fabrication of singlemode Si_3N_4 strip waveguide in 600–1000 nm wavelength range. Finally we report the first demonstration of the GCs at near-infrared (NIR) (850–950 nm) for Si_3N_4 wires and present the coupling efficiency and its dependence on the wavelength, angle and etch depth of the grating and compare with the theoretical results.

Manuscript received June 17, 2012; revised August 4, 2012; accepted August 6, 2012. Date of publication August 10, 2012; date of current version September 12, 2012. This work was supported in part by a European Research Council InSpectra Advanced Grant.

A. Z. Subramanian, S. Selvaraja, A. Dhakal, K. Komorowska, and R. Baets are with the Photonics Research Group, Center for Nano and Biophotonics, Ghent University, Ghent 9000, Belgium (e-mail: ananth.subramanian@intec.ugent.be; shankar@intec.ugent.be; ashim.dhakal@intec.ugent.be; katarzyna.komorowska@intec.UGent.be; roel.baets@intec.ugent.be).

P. Verheyen is with IMEC, Leuven 3001, Belgium (e-mail:verheyen@imec.be).

Color versions of one or more of the figures in this letter are available online at http://ieeexplore.ieee.org.

Digital Object Identifier 10.1109/LPT.2012.2212881

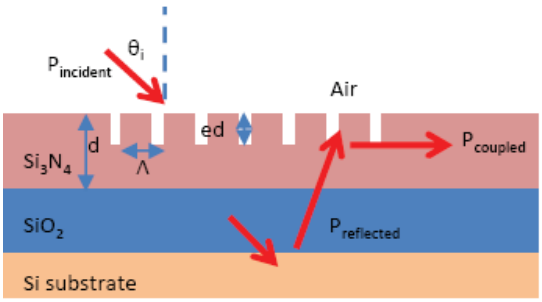

Fig. 1. Schematic diagram of the Si_3N_4 GC. Light is incident ($P_{incident}$) at θ_i angle and coupled through GC of different etch-depth (ed) into the Si_3N_4 waveguide ($P_{coupled}$). The period (Λ) of the GC and Si_3N_4 thickness are fixed at 630 and 220 nm, respectively.

II. Waveguide and Grating Coupler Design

For designing waveguides, Fimmwave (PhotonDesign) waveguide mode solver was used for simulations. A cross-section of 220 × 500 nm was used to define the core of Si_3N_4 waveguide. For this dimension, the Si_3N_4 waveguide was singlemode in 600–1000 nm wavelength range. The gratings were designed for transverse electric (TE) polarization with maximum efficiency around 900 nm, using CAMFR, an eigenmode expansion tool [10]–[11]. The GC period, fill factor (pitch/period) and number of periods was fixed at 630 nm, 0.5 and 20, respectively. The etch depth of GCs and incident angle were left as free parameters to maximize the coupling efficiency. A schematic diagram of the GC is shown in Fig. 1.

Two types of GCs were designed-linear GC (LGC) and focused GC (FGC). The schematics of both GCs (snapshots from the mask design) are shown in Fig. 2. In case of LGC,

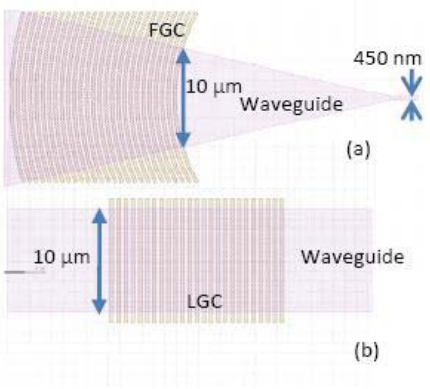

Fig. 2. Snapshots from the mask design showing (a) FGC and (b) LGC defined on top of 10-μm Si_3N_4 waveguide. The period was fixed at 630 nm.

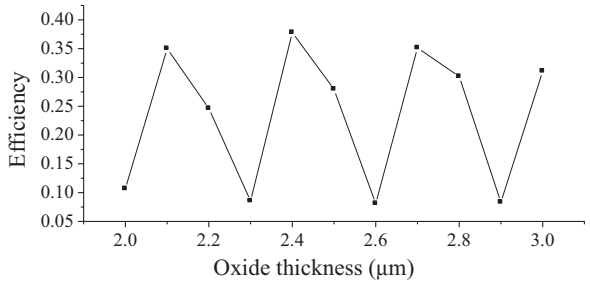

Fig. 3. Effect of buried oxide thickness on the GC efficiency as calculated by CAMFR.

two GCs at either end of the waveguide were defined on a 10 μm wide waveguide which was adiabatically tapered down to a 500 nm wire. The total length of the waveguide was 4 mm. A FGC focuses the light directly from a 10 μm wide waveguide to a 450 nm wide wire. The total length of the waveguide was 6 mm.

The underlying oxide thickness has a major influence on the coupling efficiency. Its value is chosen in such a way that the downward radiated light which gets reflected at the oxide/substrate interface ($P_{reflected}$ in Fig. 1) interferes constructively with the direct upward radiated light. This effect is depicted in Fig. 3 for the central wavelength (900 nm) of the coupler. Based on this result the oxide thickness was fixed at 2.4 μm.

III. Si_3N_4 Waveguide Fabrication and Characterization

For the fabrication, a 200 mm bare Si wafer is used as the substrate. PECVD is used to first deposit 2.4 μm of silicon dioxide (SiO_2) followed by $\sim$220 nm thick Si_3N_4 deposition on top. The SiH_4, N_2 and NH_3 gas flows were optimized for Si_3N_4 deposition at 400 °C, which ensured CMOS back-end compatibility. The deposited thin film was characterised using a prism coupling method at 633 nm (He–Ne laser) for the TE polarization. The light was coupled into the waveguide using a rutile prism into the fundamental mode of the Si_3N_4 waveguide. The index measurements were done at different places on the sample to check the homogeneity of the deposited thin film and averaged.

After the layer deposition, the waveguide and the GCs were patterned by using 193 nm optical lithography and reactive ion etch process. The waveguide was deeply etched (220 nm deep), and GCs were defined with different etch depths by controlling the etch duration. Photoresist was used as an etch mask for both the etch processes. After dry etching, the wafers were cleaned by using oxygen plasma and a wet chemical process. The widths of the waveguides were in the range of 500 $\pm$ 30 nm. Finally, some of the wafers were covered with 1.5 μm of SiO_2 using PECVD process. Since Si_3N_4 does not have any absorption band near 900 nm wavelength band, therefore no heat treatment was applied to the Si_3N_4 samples. At the end, the dies were cleaved from the wafer for optical characterization.

The propagation loss in the 500 nm wide wire was measured by cutback method using spiral waveguides with different lengths (1, 2, 4 and 7 cm) and a bend radius of 10 μm. These measurements were performed for the TE polarization using a tunable laser source emitting in the range 890–910 nm and a singlemode fibre at this wavelength range. GC measurements were performed by coupling unpolarized light from a tungsten halogen white light source (400–1700 nm) using a singlemode fibre into the Si_3N_4 waveguides. Another similar fibre is positioned above the output GC to collect the light into an optical spectrum analyzer. Both fibres were mounted on a goniometer-controlled stage to change the tilt angle. The coupling efficiency was determined from the fibre-to-fibre transmission. The position of the fibre was optimized for the maximum transmission.

IV. Results and Discussion

The prism coupling experiment yielded a refractive index of 2.043 $\pm$ 0.005 and a good uniformity with $<$ 1% variation across the wafer. The waveguide losses in the 500 nm wires were measured (@ 900 nm) for different dies from different wafers for checking the uniformity of the fabricated devices. The unclad and clad waveguides yielded a loss of 3.5 $\pm$ 1.7 dB/cm and 2.8 $\pm$ 0.6 dB/cm, respectively.

The GC efficiency (theoretical and experimental) as a function of incidence angle for 140 nm etched LGC at a wavelength of 890 nm is shown in Fig. 4. The maximum efficiency is achieved for an angle of 8° and gradually reduces for all other angles. A fairly large 1 dB angle tolerance of $\sim$4° is measured for this etch-depth. Similar optimisation was done for other etch-depths as well. The experimental measurement showed a similar trend as predicted by simulations but there was a difference in the absolute value as discussed later.

The LGC efficiency as a function of wavelength for different etch depths (70, 120, & 140 nm) is plotted in Fig. 5. The plot compares the experimental and theoretical results for the efficiencies. The efficiency plotted in Fig. 5 is calculated at optimum angle for different etch depths as shown in Fig. 4.

The efficiency of the FGC is also measured and shown in Fig. 6. The 120 nm etched FGC yielded the best efficiency of as high as $-$5.7 dB and a 1 dB bandwidth of $\sim$23 nm whereas the 220 nm etched FGC exhibited the lowest efficiency of $-$7.7 dB and a 1 dB bandwidth of $\sim$25 nm respectively.

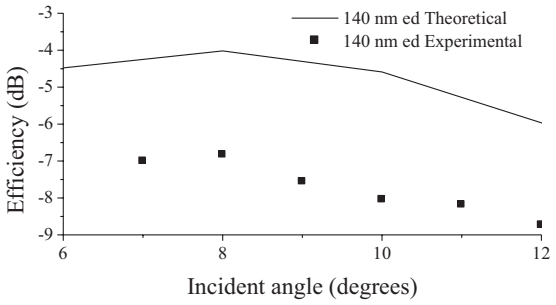

Fig. 4. LGC efficiency (theory and experiment) at 890 nm for 140 nm etched GC for different coupling angles.

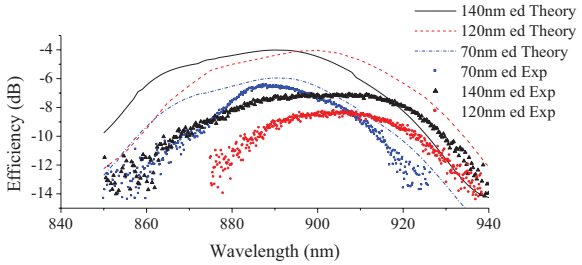

Fig. 5. LGC efficiency (theory and experiment) for different etch depths.

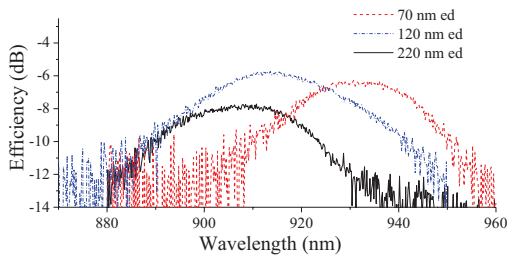

Fig. 6. FGC efficiency for 70, 120, and 220 nm etched GCs.

The grating strength (hence the effective grating length) and the reflection spectrum from the underlying substrate varies with the etch depth of the grating. For our experiments, the grating length was fixed at 20 periods and the difference in the reflection spectrum due to different etch depths leads to slight difference in the 1 dB bandwidth. Table 1 shows the efficiency and the bandwidth of FGCs with different etch depths.

The high loss in the wire is attributed to the scattering losses at the rough sidewalls as evident from the difference in the waveguide loss for clad and unclad samples. At shorter wavelengths, scattering increases and becomes more dominant and is believed to be the main source for the high waveguide loss. Therefore, further optimisation of the etch chemistry will be undertaken to smoothen the sidewall roughness and in turn reduce the losses in the waveguides.

Table 1 also compares the theoretical and experimentally determined GC efficiency and 1 dB bandwidth of the LGCs of different etch depths. The theoretical LGC efficiency calculations (dotted lines in Fig. 5) shows a maximum coupling efficiency of ~ -4 dB for the 140 nm etched grating at 890 nm and lowest (-5.9 dB) for the 70 nm etched LGC at 890 nm. Experimental measurements of the LGC for 70 nm etch depth shows reasonable agreement with the theoretical calculations.

TABLE I
EFFICIENCY AND BANDWIDTH COMPARISON FOR DIFFERENT GRATING COUPLERS AND ETCH DEPTHS

GC	Etch depth (nm)	Exp efficiency (dB)	Theoretical efficiency (dB)	Exp 1 dB bandwidth (nm)	Theoretical 1 dB bandwidth (nm)
FGC	70	-7.8	NA	25 ± 1	NA
FGC	120	-5.7	NA	24 ± 1	NA
FGC	220	-7.7	NA	21 ± 1	NA
LGC	70	-6.5	-5.9	22 ± 1	29
LGC	120	-8.2	-4	30 ± 1	32
LGC	140	-7	-4	37 ± 2	35

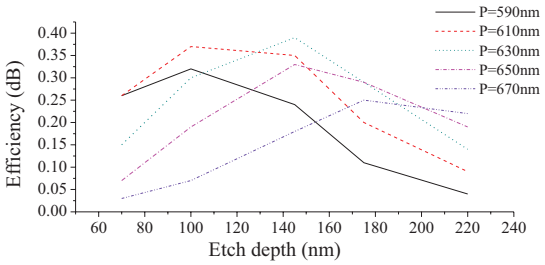

Fig. 7. Effect of period on the efficiency of GC for a given oxide thickness (2.5 μm) and 8° coupling angle.

The 70 nm etched LGC exhibited a max efficiency of -6.5 dB at 888 nm with a 1 dB bandwidth of $\sim$ 22 nm. The 140 nm etched LGC shows a slightly lower efficiency of -7 dB at 907.5 nm with a wider 1 dB bandwidth of $\sim$37 nm. The 120 nm etched LGC exhibited much lower efficiency (~ -8 dB) and a rather poor correspondence with the theoretical predictions. There is decent correspondence between the theoretical and experimental values of 1 dB bandwidth for LGC, but the big difference between the experimental values for the 120 and 140 nm etched LGC is not fully understood yet. It is believed to be caused by some anomaly in the fabricated gratings leading to deviation in the recorded signal for this grating. Also, unfortunately the direct comparison between the 140 nm LGC and FGC could not be made due to damaged waveguides in the case of FGC.

The discrepancy between the experiment and theoretical results are attributed to several reasons - a) the variation in the absolute value of the buried oxide thickness ($\sim$250 nm) leading to reduced efficiency as shown in fig. 2, b) these experiments were performed without using index matching fluid (IMF) and it is expected that using IMF would reduce the reflection losses and further improve the efficiency, c) for a given oxide thickness, a variation ($\pm$ 20 nm) in the targeted grating period has an effect both on the peak wavelength and the efficiency value of the GC output as shown in Fig. 7, and finally, d) just like in waveguides, the current etch recipe is also believed to yield rough sidewalls in the GCs leading to excess scattering loss and contributes to a lower GC efficiency.

It is worthwhile to mention here that Si_3N_4 is a deposited material and therefore it is possible to further boost the

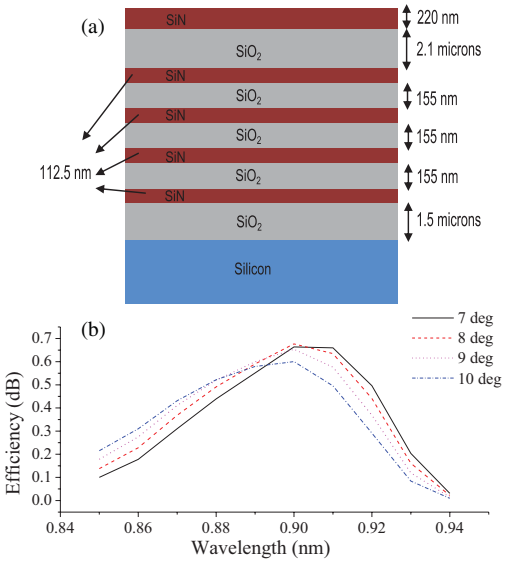

Fig. 8. (a) Si_3N_4 GC with DBR reflector and (b) simulated results at different coupling angles. The Si_3N_4 and SiO_2 thicknesses are fixed at 112.5 and 155 nm, respectively. The top oxide thickness is fixed at 2.1 μm.

efficiency by depositing a metallic mirror [2] or distributed Bragg reflectors (DBRs) underneath the grating to boost the reflection of the downward radiated light [5], [12]. Figure 8 (top) depicts a design for a DBR reflector consisting of three alternating stacks of Si_3N_4 (112.5 nm) and SiO_2 (115 nm) of different thickness. On top of such a stack a 2.1 μm oxide buffer layer is used to maximise the reflection of downward going wave. Fig. 8 (bottom) shows the simulated results for such a structure and the results suggest that an efficiency as high as 68% is achievable with such a design.

V. Conclusion

In conclusion, we have demonstrated GCs for the NIR wavelengths for the first time on a PECVD Si_3N_4 platform using a simple tungsten halogen white light source. The LGC partially etched to 70 nm exhibited a best coupling efficiency of -6.5 dB with a 1 dB bandwidth of 22 nm, whereas the GC etched by 140 nm showed a much wider 1 dB bandwidth of 37 nm but a slightly lower efficiency of -7 dB. The FGCs were better than LGCs and efficiency as high as -5.7 dB with a 1 dB bandwidth of 25 nm was achieved. The combination of Si_3N_4 wires and grating couplers enables miniature spectroscopic devices with easy accessibility to the outside world at shorter wavelengths.

Acknowledgment

The authors would like to acknowledge Dr. J. Gates, University of Southampton for their prism coupling set up. They would also like to thank IMEC's p-line and J. Wouters for the fabrication of the Si_3N_4 waveguides.

References

[1] T. Shoji, T. Tsuchizawa, T. Watanabe, K. Yamada, and H. Morita, "Low loss mode size converter from 0.3 μm square Si wire waveguides to singlemode fibres," *Electron. Lett.*, vol. 38, no. 25, pp. 1669–1670, 2002.

[2] F. Van Laere, *et al.*, "Compact and highly efficient grating couplers between optical fiber and nanophotonic waveguides," *J. Lightw. Technol.*, vol. 25, no. 1, pp. 151–156, Jan. 2007.

[3] D. Taillaert, W. Bogaerts, P. Dumon, D. Van Thourhout, and R. Baets, "Bridging the gap between nanophotonic waveguide circuits and single mode optical fibers using diffractive grating structures," *J. Nanosci. Nanotechnol.*, vol. 10, no. 3, pp. 1551–1562, 2010.

[4] S. Ghosh, C. R. Doerr, and G. Piazza, "Aluminum nitride grating couplers," *Appl. Opt.*, vol. 51, no. 17, pp. 3763–3767, 2012.

[5] C. R. Doerr, L. Chen, Y. K. Chen, and L. L. Buhl, "Wide bandwidth silicon nitride grating coupler," *IEEE Photon. Technol. Lett.*, vol. 22, no. 19, pp. 1461–1463, Oct. 1, 2010.

[6] I. M. White, J. Gohring, and X. Fan, "SERS-based detection in an optofluidic ring resonator platform," *Opt. Express*, vol. 15, no. 25, pp. 17433–17442, 2007.

[7] A. Gorin, A. Jaouad, E. Grondin, V. Aimez, and P. Charette, "Fabrication of silicon nitride waveguides for visible-light using PECVD: A study of the effect of plasma frequency on optical properties," *Opt. Express*, vol. 16, no. 18, pp. 13509–13516, 2008.

[8] J. N. Milgram, J. Wojcik, P. Mascher, and A. P. Knights, "Optically pumped Si nanocrystal emitter integrated with low loss silicon nitride waveguides," *Opt. Express*, vol. 15, no. 22, pp. 14679–14688, 2007.

[9] A. Gondarenko, J. S. Levy, and M. Lipson, "High confinement micron-scale silicon nitride high Q ring resonator," *Opt. Express*, vol. 17, no. 14, pp. 11366–11370, 2009.

[10] D. Taillaert, P. Bienstman, and R. Baets, "Compact efficient broadband grating coupler for silicon-on-insulator waveguides," *Opt. Lett.*, vol. 29, no. 23, pp. 2749–2751, 2004.

[11] P. Bienstman and R. Baets, "Optical modelling of photonic crystals and VCSELs using eigenmode expansion and perfectly matched layers," *Opt. Quantum Electron.*, vol. 33, nos. 4–5, pp. 327–341, 2001.

[12] S. Selvaraja, *et al.*, "Highly efficient grating coupler between optical fiber and silicon photonic circuit," in *Proc. CLEO 2009*, pp. 1–3, paper CTuC6.